Mechanisms Underlying Cardiac Vulnerability to Electric Shocks within the Three-Dimensional Volume of the Rabbit Ventricles

T Maharaj[1], B Rodriguez[1], R Blake[2], NA Trayanova[2], DJ Gavaghan[1]

[1]University of Oxford, Oxford, UK
[2]Tulane University, New Orleans, LA, USA

Abstract

The goal of this study is to investigate the contribution of transmural heterogeneities in action potential duration (APD) to the mechanisms of cardiac vulnerability to electric shocks, in an attempt to better understand the mechanisms behind defibrillation failure. This study used a three-dimensional, geometrically accurate finite element bidomain model of the rabbit ventricles. Transmural heterogeneities in ionic currents were incorporated based on experimental data to generate the transmural APD profile recorded in adult rabbits during pacing. Results reveal that the upper limit of vulnerability (ULV) is 30.5V/cm and the vulnerable window (VW) extends from CI=120ms to CI=190ms. Examination of shock-end virtual electrode polarisation and postshock electrical activity reveals that increased dispersion in postshock repolarisation within the LV wall play a key role in the existence of the ULV whereas mechanisms underlying the existence of the VW are determined by shock-end refractoriness in the septum.

1. Introduction

ELECTRICAL defibrillation by the timely application of a strong electric shock is the only effective therapy against cardiac arrhythmias. However, mechanisms behind defibrillation failure are still unclear. A large body of research has demonstrated that defibrillation and vulnerability to electric shocks are strongly linked as they are driven by the same factors [1]-[3].

Recently, the use of an anatomically based computational model of stimulation/defibrillation has provided significant insight into the mechanisms of defibrillation failure in normal [8], [11], and diseased hearts [9]. However, one of the limitations of existing models is the fact that cardiac tissue is considered to be entirely homogeneous. Experimental and theoretical studies in both isolated ventricular tissue [4], and single myocytes [6] have proved that ionic properties change in the depth of the ventricular wall. In particular, three layers of functionally different cell types have been identified, namely the epicardial, endocardial and midmyocardial layers. Transmural dispersion in action potential duration (APD), which results from these changes in ionic properties, is known to modulate the arrhythmogenic substrate [10] and thus could alter defibrillation efficacy. The goal of this study is to provide insight into the mechanisms of defibrillation failure by investigating the mechanisms of cardiac vulnerability to electric shocks using an anatomically accurate [15] 3D rabbit ventricular computer model, which for the first time incorporates transmural heterogeneities in APD.

2. Methods

a. *Computational model*

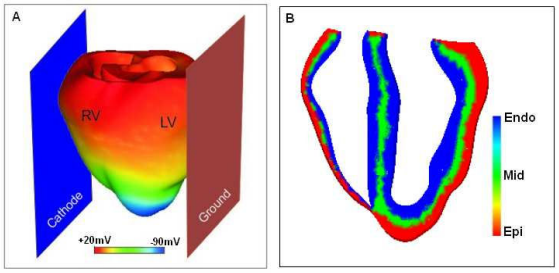

Fig.1 A) Anterior view of the rabbit ventricular model with shock electrodes showing the epicardial transmembrane potential distribution 130ms after pacing stimulation at the apex. LV=left ventricle; RV=right ventricle. B) Distribution of epicardial, endocardial and midvocardial lavers within the intact ventricles.

We used a model that incorporates realistic ventricular geometry and fibre orientation and includes representation of the conductive medium surrounding the ventricles [8]. Electrical activity in the myocardium was simulated using the bidomain equations. Membrane kinetics were represented by the Luo-Rudy dynamic model modified for defibrillation [11]. Transmural heterogeneities in the transient outward current (I_{to}) and slow delayed rectifier potassium current (I_{Ks}) were incorporated based on experimental data to generate the transmural APD profile recorded in adult rabbits [7] during pacing stimulation. Endocardial, epicardial and

midmyocardial layers are represented with relative thicknesses of 3:3:2 (Fig. 1B) [13]. Table 1 presents the values of the maximum conductances of I_{to} [12] and I_{Ks} [13] in each layer.

	Epicardium	Midmyocardium	Endocardium
G_{To} (mS/μF)	0.5	0.2125	0
G_{Ks} (mS/μF)	0.75	0.25	0.3

Table 1: Maximum conductance of I_{to} [12] and I_{Ks} [13].

b. Vulnerability grid

The rabbit ventricles were paced at the apex at a basic cycle length of 250ms. After 7 paced beats, 8ms truncated exponential monophasic shocks of varying strengths (3.81 - 30.46 V/cm) and coupling intervals (CI) between 100 and 200ms were applied via large planar electrodes located at the boundaries of the perfusing bath (Fig. 1A), in order to determine the upper limit of vulnerability (ULV) and the vulnerable window (VW). Shocks were delivered between a cathode near the right ventricle (RV), and a grounding electrode near the left ventricle (LV). CI_{max} refers to the highest CI for which an arrhythmia was induced. Shock strength (SS) refers to the leading edge value of the applied electric field.

3. Results

a. Transmural dispersion in APD

Fig. 2A illustrates the APD distribution across a transmural slice of the ventricular model. Action potential duration is measured at 90% repolarisation. Consistent with previous experimental [7] and theoretical studies [14],

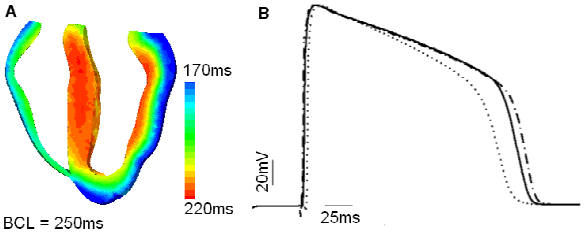

Fig. 2. Dispersion in action potential duration. A) APD distribution in a transmural slice through the ventricles showing an APD map measured at 90% repolarisation. B) Time course of the AP in epicardial (dotted line), midmyocardial (solid line) and endocardial (dashed line) layers within the LV wall in the heterogeneous ventricular model.

transmural heterogeneities in I_{to} and I_{Ks} result in a marked dispersion of APD across the LV, RV walls and the septum with APDs ranging from 170ms to 220ms in our simulations as well as in experimental recordings [7]. As Fig. 2A shows, the longest APDs are recorded in the septum and in the endocardium of the LV free wall.

Fig. 2B illustrates the time course of action potentials in an epicardial node (dotted line), a midmyocardial node (solid line) and an endocardial node (dashed line) located in the middle of each respective layer in the LV. Fig. 2B shows that APD is shorter in the midmyocardium than in the endocardium, in spite of the fact that G_{Ks} (defined in Table 1) is lower in the midmyocardium than in the endocardium. This modulation of APD is due to the electrotonic interaction between the three layers that acts to shorten the midmyocardial AP and to prolong the epicardial and endocardial APs [14].

b. Area of vulnerability

The ULV is 30.46V/cm and the VW extends from CI=120ms to CI=190ms. In order to elucidate the mechanisms underlying the ULV and the VW, we analyse the pre-shock state of the tissue, virtual electrode polarisation (VEP) [8] and the postshock electrical activity for various shock strengths and CIs.

c. Mechanisms underlying ULV

Fig. 3 shows the transmembrane potential distribution at the time of shock delivery, at shock end and following shocks of strength 30.5V/cm (i.e. the ULV, panel A) and 34.3V/cm (i.e. above the ULV, panel B) applied at CI=140ms.

Both episodes in Fig. 3 show the same pre-shock transmembrane potential distributions (Fig. 3, Pre-shock panels). Consistent with experimental optical mapping recordings [5], at shock-end, two main areas of opposite polarisation are induced on the epicardium by the shock: the RV epicardium is positively polarised while the LV epicardium is negatively polarised (Fig. 3, 0ms panels). In contrast to the surface view, the transmural views in the 0ms panels in Fig. 3 show a complex distribution of transmembrane potential in the depth of the ventricular wall, consistent with previous studies [8].

Following shock-end, similar behaviour occurs in both episodes illustrated in Fig. 3: a wavefront quickly propagates across the epicardium from apex to base. At 20ms postshock, (Fig. 3, 20ms panels, transmural views) a wavefront is initiated at the apex at the site of largest voltage gradient between oppositely polarised areas and propagates from apex to base within the LV wall.

A big difference between these two cases arises in the encircled areas in Fig. 3, 20ms panels, which eventually determines the outcome of the shock. With an increase in shock strength from 30.5V/cm to 34.3V/cm, postshock propagation is faster in Fig. 3B (SS>ULV) than in Fig. 3A (SS=ULV). As a consequence of this, the extent of the excitable area at 20ms postshock, is smaller in Fig. 3B, than in Fig. 3A (Fig 4, 20ms panels, encircled areas). This finding has been quantified by determining the percent of myocardial nodes experiencing potentials below -50mV in the encircled areas (Fig. 3A and 3B, 20ms panels).

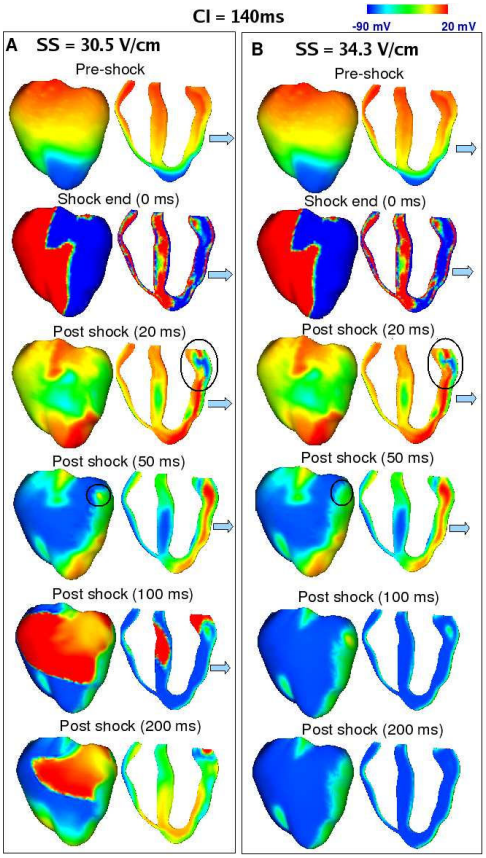

Fig. 3. Transmembrane potential distribution: pre-shock (epicardial and transmural views), at shock end (epicardial and transmural views) and the evolution of electrical activity after the shock (epicardial and transmural views) applied at CI=140ms. A) Corresponds to a shock of strength 30.5 V/cm, and B) to a shock of strength 34.3V/cm. Colour scale is saturated, i.e. transmembrane potential above 20mV and below −90mV appears red and blue, respectively.

At 20ms postshock, the amount of myocardial nodes in the encircled area, with Vm<-50mV is 33.42% for SS=30.5V/cm as compared to 24.64% for SS=34.3V/cm, indicating that there is a slightly larger excitable area ahead of the wavefront in the LV free wall for SS=ULV (Fig. 3A, 20ms panel).

For SS=ULV (Fig. 3A, 20ms panel), tissue in the LV epicardium has ample time to recover, thus providing a pathway for the postshock wavefront to break through to the epicardial surface at 50ms postshock (Fig. 3A, 50ms panel, encircled area). It then continues towards the septum and the RV tissue, which have already recovered from shock-induced positive polarisation (Fig. 3A, 100ms panel) which ultimately allows for the establishment of a re-entrant circuit. In contrast, when shock strength is increased above the ULV, (Fig.3B, 50ms panel), the epicardium does not have sufficient time to recover excitability and shortly thereafter, the wave is blocked surrounded by refractory tissue and no arrhythmia is induced (Fig 3B, 100ms panels).

d. Mechanisms underlying the vulnerable window

In order to understand the mechanism by which shock timing (i.e. CI) affects cardiac vulnerability to electric shocks, in Fig. 4, we analyse the pre-shock state, VEP and postshock electrical activity applied at three CIs, i.e. CI=140ms (Fig. 4A), 180ms (Fig. 4B) and 200ms (Fig. 4C). Shocks are applied at the SS at which the VW occurs, i.e. SS=7.62V/cm.

In Fig. 4, the pre-shock state of the tissue becomes more negatively polarised with increasing CI (Fig. 4, pre-shock panels). As a result, at long CIs (i.e. CI=200ms), the septum at shock end becomes strongly positively polarised (Fig. 4C, 0ms panels). The changes induced in septal VEP by varying shock timing ultimately determine the outcome of shocks, and thus explains the existence of the VW.

For CIs within VW, at shock-end, septal tissue is weakly depolarised (Fig. 4A, 0ms panel) or repolarised (Fig. 4B, 0ms panel). As a consequence of this, excitable areas within the LV wall and the septum are still present at 20ms postshock (Fig. 4A, 4B, 20ms panels), allowing propagation and ultimately allowing for the establishment of a re-entrant circuit (Fig. 4A, 4B, 100ms and 200ms panels). In contrast, for CI>$CI_{max,}$ (Fig. 4C), the extent of tissue at shock-end polarised above +20mV increases above 33% of myocardial volume. At 20ms postshock, a wavefront propagates quickly through the post-shock excitable region in the LV free wall. But, the wavefront is then surrounded by uniformly depolarised tissue (Fig. 4C, 20ms panel), which leads to propagation block.

4. Discussion and conclusions

In this study, an anatomically accurate 3D computer model of the rabbit ventricles, which for the first time incorporates transmural heterogeneities in APD, was used to provide insight into the mechanisms of cardiac vulnerability to electric shocks. This model presented a unique opportunity to explore electrical events that occur within the 3D volume of the ventricles with high spatial-temporal resolution before, during and after the application of electrical shocks in the depth of the ventricular wall, which is not achievable via any imaging techniques thus far.

Insight provided by the simulations reveals that the ULV is determined by postshock behaviour within the LV free wall. Our results show that the presence of transmural heterogeneities and in particular the fact that APD is shorter in the epicardial than in the midmyocardial layer facilitates the induction of re-entry within the LV wall.

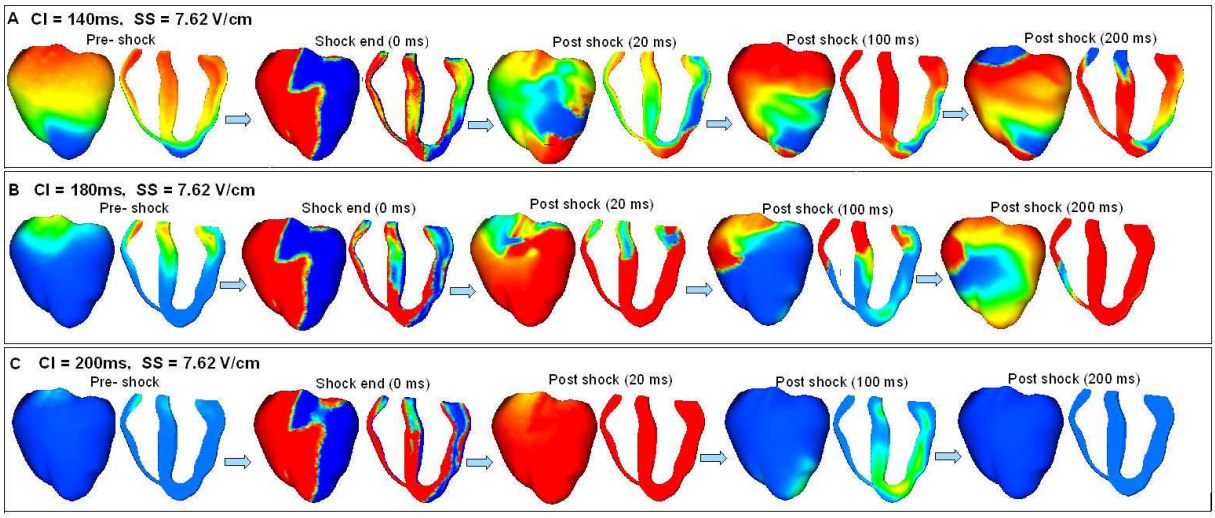

Fig. 4. Transmembrane potential distribution: pre-shock (epicardial and transmural views), at shock end (epicardial and transmural views) and the evolution of electrical activity after the shock (epicardial and transmural views) applied at SS=7.62V/cm. A) Corresponds to CI=140ms, B) to CI=180ms and C) to CI=200ms. Colour scale as in Fig. 3.

In contrast, simulation results reveal that shock-end polarisation within the septum plays a key role in the mechanisms underlying the existence of the VW. This information could aid in the design of new and more efficient protocols for cardiac defibrillation.

Acknowledgements

This work was supported by a Rhodes scholarship to T. M., the EPSRC-funded Integrative Biology e-Science pilot project (ref no: GR/S72023/01), by the EU BioSim Grant (005137) and by AHA Established Investigator Award (N.T.), and the grant HL63195 from NIH (N.T).

References

[1] Malkin RA., Idriss SF., Walker RG., and Ideker RE., Effect of rapid pacing and T-wave scanning on the relation between the defibrillation and upper-limit-of-vulnerability dose-response curves. Circulation 1995;92:1291-1299.

[2] Chen PS., Shibata N., Dixon EG., Wolf PD., et al. Activation during ventricular defibrillation in open-chest dogs. J Clin Invest. 1986 ; 77(3): 810–823.

[3] Chen PS., Feld GK., Mower MM., Peters BB. Effects of pacing rate and timing of defibrillation shock on the relation between the defibrillation threshold and the upper limit of vulnerability in open chest dogs. J Am Coll Cardiol. 1991; 18:1555-1563.

[4] Antzelevitch C., Shimizu W, Yan GX, et al. The M cell: its contribution to the ECG and to normal and abnormal electrical function of the heart. J Cardiovasc Electrophysiol. 1999;10(8):1124-52.

[5] Efimov IR., Aguel F., Cheng Y., Wollenzier B., et al. Virtual electrode polarization in the far field: implications for external defibrillation. Am J Physiol Heart Circ Physiol. 2000; 279:1055-1070.

[6] McIntosh MA, Cobbe SM, Smith GL. Heterogeneous changes in action potential and intracellular Ca2+ in left ventricular myocyte sub-types from rabbits with heart failure. Cardiovasc Res. 2000 ;45(2):397-409.

[7] Idriss SF. and Wolf PD. Transmural action potential repolarisation heterogeneity develops postnatally in the rabbit. J. Cardiovas Electrophysiol. 2004;15:795-801.

[8] Trayanova N., Eason J. and Aguel F. Computer simulations of cardiac defibrillation: A look inside the heart. Computer Visual Science 2002;4:259 – 270.

[9] Rodríguez B, Tice B, Eason J, Aguel F, Trayanova N. Cardiac vulnerability to electric shocks during phase 1A of acute global ischemia. Heart Rhythm 2004:695-703.

[10] Antzelevitch C., Fish J. Electrical heterogeneity within the ventricular wall. Bas Res Cardiol. 2001;96:517-527.

[11] Ashihara T. and Trayanova NA. Asymmetry in membrane responses to electric shocks: Insights from bidomain simulations. Biophysical Journal 2004;87: 2271-2282.

[12] Dumaine R., Towbin JA., Brugada P., et al. Ionic mechanisms responsible for the electrocardiographic phenotype of the Brugada syndrome are temperature dependent. Circ. Res. 1999;85: 803-809.

[13] Saucerman JJ., Healy SN., Belik ME., et. al. Proarrhythmic consequences of a KCNQ1 AKAP-binding domain mutation computational models of whole cells and heterogeneous tissue. Circ. Res. 2004;95:1216.

[14] Sampson KJ. and Henriquez CS. Simulation and prediction of functional block in the presence of structural and ionic heterogeneity. Am J Physiol. 2001;281:2597-2603.

[15] Vetter FJ. and McCulloch AD. Three-dimensional analysis of regional cardiac function: a model of rabbit ventricular anatomy. Prog Biophys Mol Biol. 1998;69: 157-183.

Address for correspondence
Name Thushka Maharaj
Postal address Computing Laboratory,
Oxford,
OX13QD,
UK.